Thermally activated escape from the zero-voltage state in long Josephson junctions

M. G. Castellano* and G. Torrioli*
Istituto di Elettronica dello Stato Solido, CNR, via Cineto Romano 42, I-00156 Roma, Italy

C. Cosmelli,* A. Costantini, and F. Chiarello*
Dipartimento di Fisica, Università di Roma ''La Sapienza,'' P.le Aldo Moro 5, I-00185 Roma, Italy

P. Carelli* and G. Rotoli
Dipartimento di Energetica, Università dell'Aquila, Monteluco di Roio, I-67040 L'Aquila, Italy

M. Cirillo*
Dipartimento di Fisica, Università di Roma Tor Vergata, I-00133 Roma, Italy

R. L. Kautz
National Institute of Standards and Technology, 325 Broadway, Boulder, Colorado 80303
(Received 26 April 1996)

We have measured the rate of thermally induced escape from the zero-voltage state in long Josephson junctions of both overlap and in-line geometry as a function of applied magnetic field. The statistical distribution of switching currents is used to evaluate the escape rate and derive an activation energy ΔU for the process. Because long junctions correspond to the continuum limit of multidimensional systems, ΔU is in principle the difference in energy between stationary states in an infinite-dimensional potential. We obtain good agreement between calculated and measured activation energies for junctions with lengths a few times the Josephson penetration depth λ_J. [S0163-1829(96)01145-9]

I. INTRODUCTION

The classical process of thermal excitation over an energy barrier was studied theoretically by Kramers[1] in terms of a simple activation model in which the relevant parameters are an angular attempt frequency ω_A and an activation energy equal to the energy barrier ΔU. The rate of escape Γ over the barrier is given by

$$\Gamma = (\omega_A/2\pi)\exp(-\Delta U/k_B T), \tag{1}$$

where k_B is Boltzmann's constant and T is the temperature. Analyzed in terms of this simple and effective theory, measurement of thermal escape from the zero-voltage state of a Josephson tunnel junction has attracted continuing attention since the early experiments performed by Fulton and Dunkleberger.[2] For small-area junctions, the potential energy of the system is a function of a single variable ϕ, the difference in phase between the macroscopic wave functions describing the superconducting electrons in the junction electrodes. The simplicity of this one-dimensional Josephson potential has motivated both theoretical[3–9] and further experimental[10–15] investigations of escape in the classical regime. The one-dimensional limit has also been explored in the quantum regime with studies of both macroscopic quantum tunneling[16–20] and the effect of energy-level quantization on escape from the zero-voltage state.[21–24] During the same period, the study of thermally activated escape was extended to encompass a Josephson system, the dc superconducting quantum interference device (SQUID), in which the potential energy depends on the phases ϕ_1 and ϕ_2 of two junctions.[25–29] This work demonstrated good agreement with extensions of Kramers's theory to multidimensional potentials.[30–32]

In this paper, we present the results of experiments on thermally activated escape from the zero-voltage state in long Josephson junctions. In a long junction, one physical dimension, say, the y dimension, is much shorter than the Josephson penetration depth λ_J, and the phase difference ϕ depends only on the coordinate x associated with the long dimension, which is typically much greater than λ_J. In long junctions, $\phi(x,t)$ satisfies the sine-Gordon equation, a partial differential equation in space and time.[33,34] Thus, in exploring thermal escape in long junctions, we confront the Kramers problem in the continuum limit of multidimensional systems. This limit has been considered from a theoretical point of view by several authors,[35–38] who developed formal expressions for the nucleation of fluxon-antifluxon pairs in junctions of infinite length, both in the thermal and the macroscopic quantum tunneling regimes. In our experiments, the junction length is finite, typically a few times λ_J, and escape can be analyzed using a simple theory that again expresses the escape rate in terms of an attempt frequency and an activation energy. As in short junctions, the activation energy is the difference in potential energy between a saddle point and a potential minimum. However, the results we obtain for long junctions contrast sharply with those for short junctions.

The experiments reported here were performed on junctions having the two geometries shown in Fig. 1: an overlap junction without a ground plane and an in-line junction with a ground plane. The behaviors of both types of junction were explored in the presence of a magnetic field applied in the

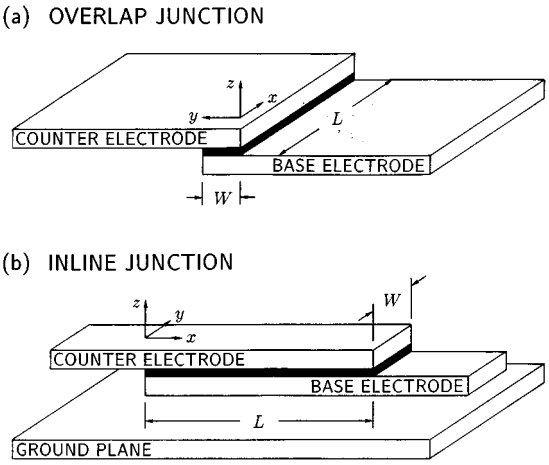

FIG. 1. Ideal geometry of the (a) overlap and (b) in-line junctions.

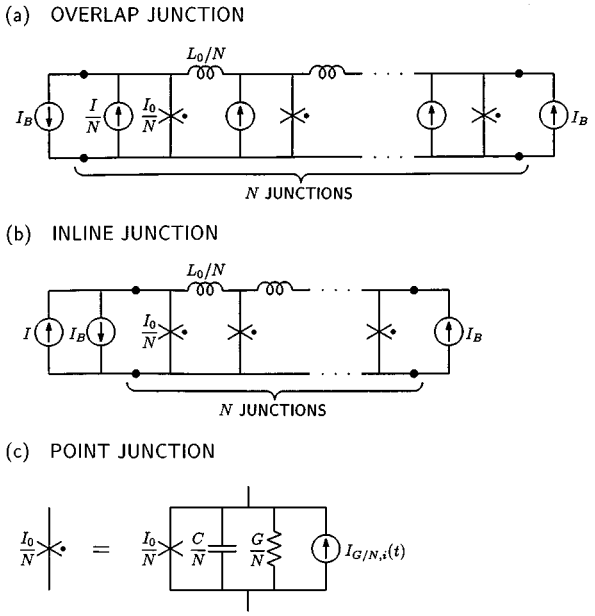

FIG. 2. Circuit models representing the (a) overlap and (b) in-line junctions in terms of discrete elements, with the point junction defined as in (c).

y direction. Following Fulton and Dunkleberger,[2] we measured the activation energy for escape from the zero-voltage state by recording the bias currents I at which the junction switched to the voltage state in a series of trials. In each trial, the junction is initialized in the zero-voltage state and the bias current is increased from zero at a constant rate $\dot{I}$ until switching occurs. Thermally activated switching occurs primarily at bias levels near the critical current I_c, where the energy barrier ΔU is comparable to the thermal energy $k_B T$. Thus, our experiments determine the activation energy only for I near I_c. In this limit, the asymptotic dependence of ΔU on I proves to be virtually identical in form to that of a short junction, but its magnitude is scaled by a factor that depends on the junction length and the applied magnetic field. Analyzed on this basis, the experimentally measured activation energies agree well with theory.

The remainder of this paper is organized as follows. In Sec. II, we develop a theory for thermally induced escape from the zero-voltage state in long overlap and in-line junctions and present numerical results for the activation energy at bias currents near the critical current. Monte Carlo simulations, presented in Sec. III, are used to confirm the basic validity of this theory, and experimental results are described and compared with theory in Sec. IV.

II. THEORY

Although a long junction is in principle a continuum system having an infinite number of degrees of freedom, junctions of finite length are well approximated in practice by a finite number of coordinates. Thus, escape from the zero-voltage state in long junctions can usually be treated as a multidimensional escape problem without passing to the continuum limit. Here we calculate the activation energy using the continuum limit but consider just a few degrees of freedom in estimating the attempt frequency. For the experiments in question, thermal energies are much greater than the level spacing of the attracting well, and so macroscopic quantum tunneling can be neglected. Our calculations are also restricted to the limit of weak damping realized in the experiment.

A. Long-junction models

Circuit models representing the overlap and in-line junctions in terms of discrete elements are shown in Fig. 2. Here, a long junction is divided into N point junctions of critical current I_0/N connected in parallel by inductors L_0/N, where $I_0 = WLJ_c$ is the critical current ideally expected for a junction of width W, length L, and critical-current density J_c, and $L_0 = \mu_0 L(s+\lambda_1+\lambda_2)/W$ is the total inductance of a junction having a barrier of thickness s and electrodes of London penetration depths λ_1 and λ_2. As indicated in Fig. 2(c), each point junction is modeled by an ideal Josephson element shunted by a capacitance C/N, a conductance G/N, and a Johnson noise source $I_{G/N,i}(t)$. Here, $C = \epsilon\epsilon_0 WL/s$ is the total capacitance of the junction (where ϵ is the relative dielectric constant of the barrier), G is the total subgap conductance, and the current source $I_{G/N,i}(t)$ is a white Gaussian noise source associated with the conductance of the ith point junction. Because the Johnson noise of distinct point junctions is uncorrelated, the autocorrelation function is

$$\langle I_{G/N,i}(t_1) I_{G/N,j}(t_2)\rangle = (2k_B TG/N)\,\delta_{ij}\,\delta(t_1 - t_2), \quad (2)$$

where δ_{ij} is a Kronecker delta and $\delta(t_1 - t_2)$ is a Dirac delta function. In the overlap junction, the dc bias is uniformly distributed over the junction length and a current source I/N is associated with each point junction. In the in-line junction, the presence of a ground plane leads to an equivalent circuit in which all of the bias current is injected at one end of the junction. In both cases, the applied magnetic field B is represented by current sources $I_B = WB/\mu_0$ that inject current at one end of the junction and withdraw it at the other end. These circuits accurately model the ideal overlap and in-line junctions in the limit $N \to \infty$.

The circuit models of Fig. 2 lead directly to partial differential equations of the sine-Gordon form in the continuum limit. Introducing the dimensionless variables $x'=x/\lambda_J$ and $t'=\omega_0 t$, where $\lambda_J=[2\pi\mu_0 J_c(s+\lambda_1+\lambda_2)/\Phi_0]^{-1/2}$ is the Josephson penetration depth, $\omega_0=(2\pi I_0/\Phi_0 C)^{1/2}$ is the zero-field plasma frequency, and $\Phi_0=h/2e$ is the flux quantum, we obtain for an overlap junction an equation for the phase $\phi(x',t')$ of the form

$$\phi_{t't'}-\phi_{x'x'}+\alpha\phi_{t'}+\sin\phi=\gamma+\xi(x',t') \quad \text{(overlap)}, \tag{3}$$

with the boundary conditions

$$\phi_{x'}(0,t')=\phi_{x'}(l,t')=\eta \quad \text{(overlap)}, \tag{4}$$

where subscripts indicate partial derivatives, $\alpha=G(2\pi I_0 C/\Phi_0)^{-1/2}$ is the normalized conductance, $\gamma=I/I_0$ is the normalized bias current, $l=L/\lambda_J$ is the normalized junction length, $\eta=2\pi\lambda_J(s+\lambda_1+\lambda_2)B/\Phi_0$ is a dimensionless magnetic field, and ξ is a dimensionless noise current with autocorrelation function

$$\langle\xi(x_1',t_1')\xi(x_2',t_2')\rangle=(4\pi l\alpha k_B T/\Phi_0 I_0)\,\delta(x_1'-x_2')\,\delta(t_1'-t_2'). \tag{5}$$

Equations (3)–(5) completely define the dynamics of a noise-affected overlap junction in the presence of an applied magnetic field and a dc bias. The analogous equation of motion for an in-line junction is

$$\phi_{t't'}-\phi_{x'x'}+\alpha\phi_{t'}+\sin\phi=\xi(x',t') \quad \text{(in-line)}, \tag{6}$$

with the boundary conditions

$$\phi_{x'}(0,t')=\eta-\gamma l, \quad \phi_{x'}(l,t')=\eta \quad \text{(in-line)}. \tag{7}$$

Our objective in the remainder of this section is to determine the rate for thermally induced escape from the zero-voltage state for these two systems in the limit of weak damping ($\alpha\ll 1$).

B. Short-junction limit

Before considering truly long junctions with $L>\lambda_j$ or $l>1$, we examine the short-junction limit $l\ll 1$, with the product ηl of magnetic field and junction length held fixed. In this limit, the point junctions that model a long junction are tightly coupled by small inductances, but the magnetic field is sufficient to produce a change in phase of $\phi(l)-\phi(0)=\eta l$ from one end of the junction to the other. As a result, the point-junction phases are splayed but always advance in unison, and the short junction is equivalent to a point junction with a critical current I_c less than I_0. In the following, we use I_c or $\gamma_c=I_c/I_0$ to represent the general case of the critical current of a noise-free junction in the presence of a magnetic field. In the short-junction limit of both the overlap and in-line geometries, we have[39]

$$I_c/I_0=\gamma_c=\left|\frac{\sin(\eta l/2)}{\eta l/2}\right| \quad \text{(short)}. \tag{8}$$

If a spatially averaged phase variable $\overline{\phi}$ is appropriately selected, the equation of motion for a short junction takes the form

$$\overline{\phi}_{t't'}+\alpha\overline{\phi}_{t'}+\gamma_c\sin\overline{\phi}=\gamma+\overline{\xi}(t'), \tag{9}$$

where $\overline{\xi}$ is the spatially averaged noise current with autocorrelation

$$\langle\overline{\xi}(t_1')\overline{\xi}(t_2')\rangle=(4\pi\alpha k_B T/\Phi_0 I_0)\,\delta(t_1'-t_2'). \tag{10}$$

Equations (9) and (10) describe the noise-affected behavior a short junction of either overlap or in-line geometry in a form equivalent to a point junction.

The dynamics of the system described by Eq. (9) is equivalent to that of a particle moving in a potential of the form

$$U(\overline{\phi})=E_J[(1-\cos\overline{\phi})-(\gamma/\gamma_c)\overline{\phi}], \tag{11}$$

where $E_J=\Phi_0 I_c/2\pi$ is the Josephson coupling energy associated with the critical current I_c. In $U(\phi)$, the terms $(1-\cos\phi)$ and $(\gamma/\gamma_c)\phi$ account for the energy stored in the ideal Josephson element and the energy supplied by the dc bias. This potential, often described as a washboard, consists of oscillations superposed on a constant slope. For $\gamma<\gamma_c$, the washboard has minima or attracting points at $\phi_a=\sin^{-1}(\gamma/\gamma_c)$ modulo 2π and maxima or saddle points at $\phi_s=\pi-\sin^{-1}(\gamma/\gamma_c)$ modulo 2π. Escape from the zero-voltage state occurs when thermal energy causes the system to escape from a potential minimum over an adjacent saddle and begin moving down the slope.

Escape in the limit of low temperatures ($k_B T\ll E_J$) and weak damping ($\alpha\ll 1$) was first analyzed for point junctions by Ivanchenko and Zil'berman.[3] Their result for the rate of escape can be expressed in terms of a barrier energy and an attempt time as in Eq. (1). The barrier energy is the energy difference between a potential minimum and the lowest adjacent saddle. That is, $\Delta U=U(\overline{\phi}_s)-U(\overline{\phi}_a)$ or

$$\Delta U/E_J=u_0=2[\sqrt{1-(\gamma/\gamma_c)^2}-|\gamma/\gamma_c|\cos^{-1}(\gamma/\gamma_c)] \quad \text{(short)}. \tag{12}$$

In the following, we use u to denote the ratio $\Delta U/E_J$ of barrier energy to coupling energy in general and reserve u_0 for the short-junction limit. Because we are especially interested in bias points near I_c, it is useful to note that

$$\lim_{\gamma\to\gamma_c} u_0=(4\sqrt{2}/3)(1-\gamma/\gamma_c)^{3/2}. \tag{13}$$

The attempt frequency in the underdamped limit is the frequency of natural oscillation about the potential minimum. Linearizing Eq. (9) about the equilibrium point yields

$$\omega_A=\omega_p[1-(\gamma/\gamma_c)^2]^{1/4} \quad \text{(short)}, \tag{14}$$

where $\omega_p=(2\pi I_c/\Phi_0 C)^{1/2}$ is the plasma frequency corresponding to the critical current I_c. Equations (12) and (14) define the rate of escape in the short-junction limit and serve as a basis of comparison for long-junction results.

C. Activation energy

As in a point junction, escape from the zero-voltage state of a long junction requires thermal activation over a barrier

defined by the difference in energy between a saddle and a minimum of a potential surface. Because ϕ is a continuous function of position in a long junction, the potential surface is defined on an infinite-dimensional space. Fortunately, the potential energy and the solutions $\phi_a(x')$ and $\phi_s(x')$ at minima and saddles are relatively simple to compute. In particular, $\phi_a(x')$ and $\phi_s(x')$ for an overlap junction are stationary solutions of Eq. (3) in the absence of noise. That is, for an overlap junction, the configurations corresponding to potential minima and saddles satisfy

$$-\phi_{x'x'}+\sin\phi=\gamma \quad \text{(overlap)}, \tag{15}$$

with the boundary conditions

$$\phi_{x'}(0)=\phi_{x'}(l)=\eta \quad \text{(overlap)}. \tag{16}$$

For the static solutions defined by Eqs. (15) and (16), the potential energy U of the overlap junction is given by

$$U/E_0=\frac{1}{l}\int_0^l\left[(1-\cos\phi)-\gamma\phi+\frac{1}{2}(\phi_{x'}-\eta)^2\right]dx' \quad \text{(overlap)}, \tag{17}$$

where $E_0=\Phi_0 I_0/2\pi$ is the Josephson coupling energy corresponding to the ideal critical current I_0. The terms $(1-\cos\phi)$ and $-\gamma\phi$ account for the energy stored in the Josephson elements and the energy supplied by the dc bias, while the term $\frac{1}{2}(\phi_{x'}-\eta)^2$ includes both the energy stored in the inductance L_0 and the energy supplied by the magnetic bias. For an in-line junction, $\phi_a(x')$ and $\phi_s(x')$ satisfy the equation

$$-\phi_{x'x'}+\sin\phi=0 \quad \text{(in-line)}, \tag{18}$$

with the boundary conditions

$$\phi_{x'}(0)=\eta-\gamma l, \quad \phi_{x'}(l)=\eta \quad \text{(in-line)}, \tag{19}$$

and the potential energy is

$$U/E_0=-\gamma\phi(0)+\frac{1}{l}\int_0^l\left[(1-\cos\phi)+\frac{1}{2}(\phi_{x'}-\eta)^2\right]dx' \quad \text{(in-line)}, \tag{20}$$

where the term $-\gamma\phi(0)$ accounts for energy supplied by the dc bias. Equations (15)–(20) provide a fully practical method of calculating the barrier energy $\Delta U=U(\phi_s)-U(\phi_a)$ for escape from the zero-voltage state of long junctions.

Because the boundary conditions specify $\phi_{x'}$ at $x'=0$ and l, numerical solution of Eqs. (15) and (18) relies on a shooting method, in which $\phi(0)$ is adjusted by trial and error to obtain $\phi_{x'}(l)=\eta$ upon integration from $x'=0$ to l. While this method allows $\phi_a(x')$ and $\phi_s(x')$ to be computed efficiently, it does not reveal which solutions correspond to potential minima and which to saddle points. To determine the stability, we calculate the change in U for infinitesimal deviations $\Delta\phi(x')$ from a given solution $\phi(x')$ of Eq. (15) or (18). A deviation that satisfies the required boundary conditions can be expanded in a cosine series of the form

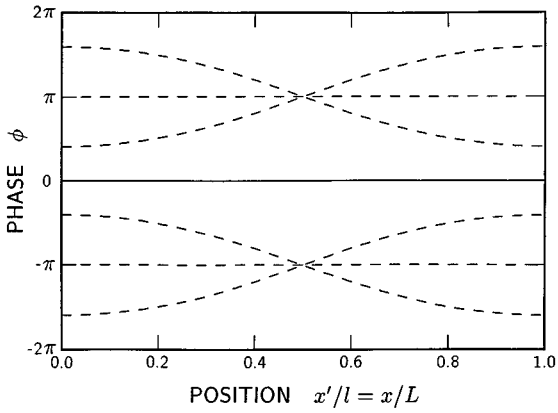

FIG. 3. Phase as a function of position for stationary solutions of either an overlap or an in-line junction of length $l=4$ in the absence of a dc or magnetic bias ($\gamma=\eta=0$). The solid line at $\phi=0$ shows a configuration corresponding to a potential minimum and dashed lines correspond to saddles.

$$\Delta\phi(x')=\sum_{m=1}^{M} a_m\cos[(m-1)\pi x'/l], \tag{21}$$

without loss of generality, provided that M is allowed to be arbitrarily large. Considering the potential $U(\phi+\Delta\phi)$ for either the overlap or in-line case, we find that the derivatives $\partial U/\partial a_m$ are identically zero if ϕ satisfies the corresponding differential equation. This result confirms that the solutions of Eqs. (15) and (18) represent minima or saddles of the energy surface. To determine stability, we consider the matrix **A** of second derivatives of the potential, defined by

$$A_{mn}=\frac{\partial^2 U}{\partial a_m\partial a_n}=\frac{E_0}{2}\left[\frac{(m-1)\pi}{l}\right]^2\delta_{mn}+\frac{E_0}{l}\int_0^l\cos\phi\cos[(m-1)\pi x'/l]\times\cos[(n-1)\pi x'/l]dx', \tag{22}$$

which applies to both overlap and in-line junctions. According to multivariate calculus, the solution $\phi(x')$ corresponds to an energy minimum if and only if the eigenvalues of **A** are all positive. Although **A** is in principle an infinite-dimensional matrix, an accurate determination of stability is obtained in practice by considering only the first few Fourier components of the deviation, and a matrix of size $M=10$ proved adequate in all cases presented here. Thus, the stability of a given solution can be readily determined.

As an example, stationary configurations for the phase of either an overlap or an in-line junction of length $l=4$ in the absence of a dc or magnetic bias ($\gamma=\eta=0$) are plotted in Fig. 3. Because Eqs. (15) and (18) are invariant with respect to a 2π shift in phase, any solution $\phi(x')$ represents an infinite set of solutions that are equivalent modulo 2π. Thus, the stable configuration plotted as a solid line at $\phi=0$ in Fig. 3 implies the existence of similar solutions at $\phi=2n\pi$. This set of solutions is fully expected since it corresponds to a situation in which all of the point junctions are at minimum energy. The dashed line at $\phi=\pi$ is also expected as the

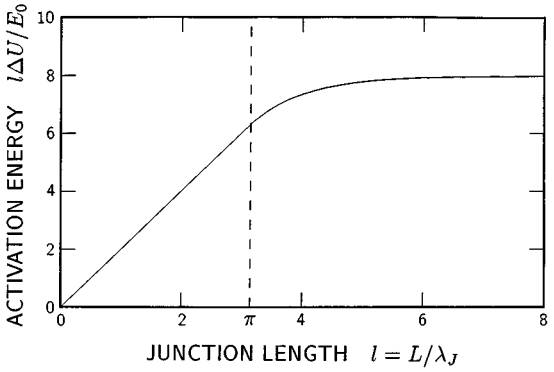

FIG. 4. Activation energy as a function of junction length for the process of moving between potential minima in the absence of a dc or magnetic bias ($\gamma = \eta = 0$). The activation energy is the same for overlap and in-line junctions.

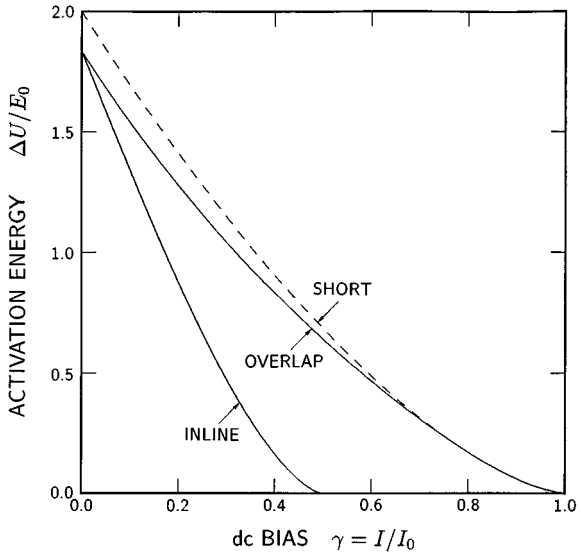

FIG. 5. Activation energy for escape from the zero-voltage state as a function of dc bias for overlap and in-line junctions of length $l = 4$ in the absence of a magnetic bias ($\eta = 0$). The critical currents of the overlap and in-line junctions are $\gamma_c = 1$ and 0.499, respectively. A dashed line shows the short-junction limit.

unstable state in which the point junctions are at maximum energy. The total energies of these two states are $U/E_0 = 0$ and 2, respectively. However, as Fig. 3 indicates, there are two additional unstable states that break the spatial symmetry of the problem. These solutions pass through $\phi = \pi$ at the midpoint of the junction but deviate from π at the ends. Both solutions of this symmetry-breaking pair have a total energy of $U/E_0 = 1.836$. They are lower in energy than the $\phi = \pi$ solution because the phase bending lowers the total energy stored in the junction elements by $0.726\,E_0$ while raising the energy stored in L_0 by only $0.562\,E_0$. The symmetry-breaking solutions thus imply the existence of saddles points between the potential minima at $\phi = 0$ and $\phi = 2\pi$ with a lower energy barrier than that afforded by the $\phi = \pi$ saddle. In this regard, the flexibility of a long junction is analogous to that of a pole vaulter who, by bending his body, is able to clear a bar without his center of mass exceeding the height of the bar.

The role of junction length in reducing the activation energy of thermally induced phase slippage is further explored in Fig. 4, where we plot ΔU as a function of l for the process of moving between potential minima in the absence of a dc or magnetic bias. Here, ΔU is normalized to $E_0/l = \Phi_0 W \lambda_J J_c/2\pi$ to avoid using a normalization that depends on length. For $l < \pi$ symmetry-breaking solutions are excluded, the saddle solution is of the form $\phi = \pi$, and the barrier energy is $\Delta U = 2E_0$. In this regime, the activation energy increases in proportion to length simply because the ideal critical current increases with length. For $l > \pi$, however, the lowest saddle point results from symmetry-breaking solutions, and the activation energy fails to increase in proportion to length. Indeed, in the limit $l \to \infty$, the activation energy approaches a constant, $l\Delta U/E_0 = 8$, which is the energy required to create a fluxon in a junction of infinite length.[39] This limit makes sense physically because a 2π phase advance can be obtained more easily by allowing a fluxon to propagate through a long junction than by requiring that all of the point junctions pass through their maximum-energy states simultaneously.

At any nonzero dc bias, a thermally induced phase slip can lead directly to the voltage state if the damping constant α is sufficiently small. Thus, for $\gamma > 0$, the barrier energy ΔU can be taken as the activation energy for escape from the zero-voltage state. As an example, we plot in Fig. 5 the activation energy as a function of γ for overlap and in-line junctions of length $l = 4$ in the absence of a magnetic field ($\eta = 0$). For comparison, the short-junction limit [Eq. (12)] is shown by a dashed line. The activation energies of both the overlap and in-line junctions coincide at $\gamma = 0$, decrease monotonically with increasing dc bias, and approach zero at their respective critical currents. The critical current γ_c is 1 for the overlap geometry, in which the bias current is spatially uniform, and 0.499 for the in-line geometry, in which the bias current is concentrated at $x' = 0$. Critical currents for an in-line junction with a ground plane were explored previously by Basavaiah and Broom.[40]

The nature of the stationary solutions that define the energy barrier in Fig. 5 changes with bias. As noted above, the overlap and in-line junctions are equivalent at $\gamma = 0$ and yield one minimum-energy solution and three saddle solutions. The three saddles persist for small values of $\gamma > 0$, but two of the saddles disappear above $\gamma = 0.787$ in the overlap junction and above $\gamma = 0.131$ in the in-line junction. Thus, in both cases, just one saddle and one minimum exist in the bias region near γ_c. This makes computation of the activation energy especially simple in the region of primary relevance to our experiments. For the overlap junction, the minimum and saddle for $0.787 < \gamma < 1$ correspond to spatially uniform solutions and the activation energy coincides with the short-junction limit. For both geometries, the minimum-energy and saddle solutions coalesce and disappear in the limit $\gamma \to \gamma_c$.

We now consider the activation energy in the presence of an applied magnetic field. Although a magnetic field does not significantly complicate the calculation of ΔU, it ensures that phase bending occurs even in the overlap geometry, where the dc bias is spatially uniform. This effect is illus-

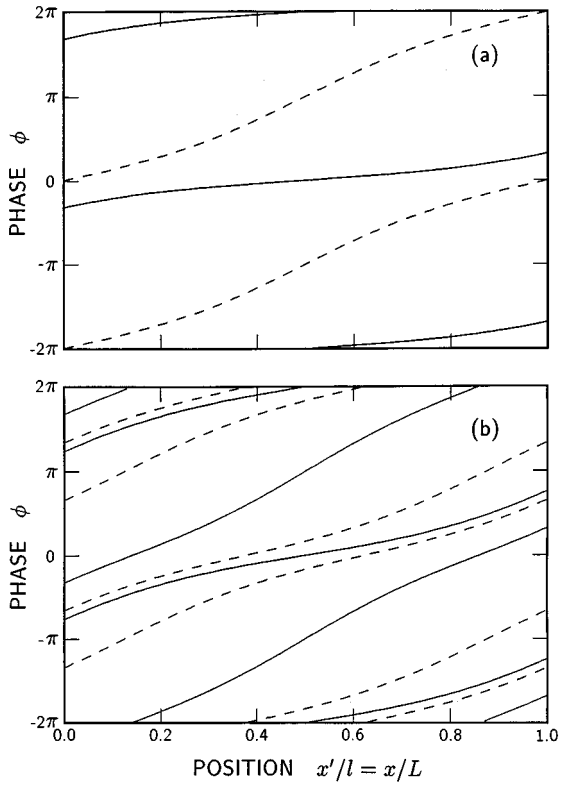

FIG. 6. Phase as a function of position for stationary solutions of an overlap junction with length $l=4$, dc bias $\gamma=0$, and magnetic fields (a) $\eta=1$ and (b) $\eta=2$. Solutions corresponding to potential minima and saddle points are plotted as solid and dashed lines.

trated in Fig. 6, which shows the phase of stationary solutions as a function of position for an overlap junction of length $l=4$ in the absence of a dc bias ($\gamma=0$). In Fig. 6(a), where $\eta=1$, the phase bending is relatively weak, and there is just one minimum-energy solution and one saddle solution. On the other hand, Fig. 6(b) shows the situation at $\eta=2$, near the first minimum of the threshold curve, where there are two minimum-energy solutions and two saddle solutions. However, the application of a dc bias again reduces the set of solutions to one minimum and one saddle well before the critical current is reached.

To examine the activation energy near the critical current for a general case, we consider overlap and in-line junctions of length $l=4$ with a magnetic field of $\eta=1$. The activation energies for this case are plotted as a function of dc bias in Fig. 7. To facilitate comparison with the short-junction limit, the dc bias and activation energies are normalized to I_c and $E_J=\Phi_0 I_c/2\pi$ rather than I_0 and $E_0=\Phi_0 I_0/2\pi$. These normalizations are advantageous because I_c is readily determined experimentally and because they lead to a universal curve for short junctions (dashed line) that is independent of magnetic field [cf. Eq. (12)]. As Fig. 7(a) indicates, however, long junctions need not follow this universal curve, and the activation energy of long junctions may be either more or less than that predicted by the short-junction limit. Nonetheless, the asymptotic behavior of $u=\Delta U/E_J$ assumes an approximate invariant form in the limit $\gamma\rightarrow\gamma_c$. That is, for junctions up to at least a few times λ_J in length, the activation energy scales approximately as $(1-\gamma/\gamma_c)^{3/2}$ in the neighborhood of the critical current, as suggested by the limiting form for short junctions given by Eq. (13). This behavior is confirmed for the case at hand by the logarithmic plot of u versus $1-\gamma/\gamma_c$ shown in Fig. 7(b). In this figure, the bias dependence of u for both the overlap and in-line junctions is represented by a straight line that confirms the 3/2 power law for γ near γ_c.

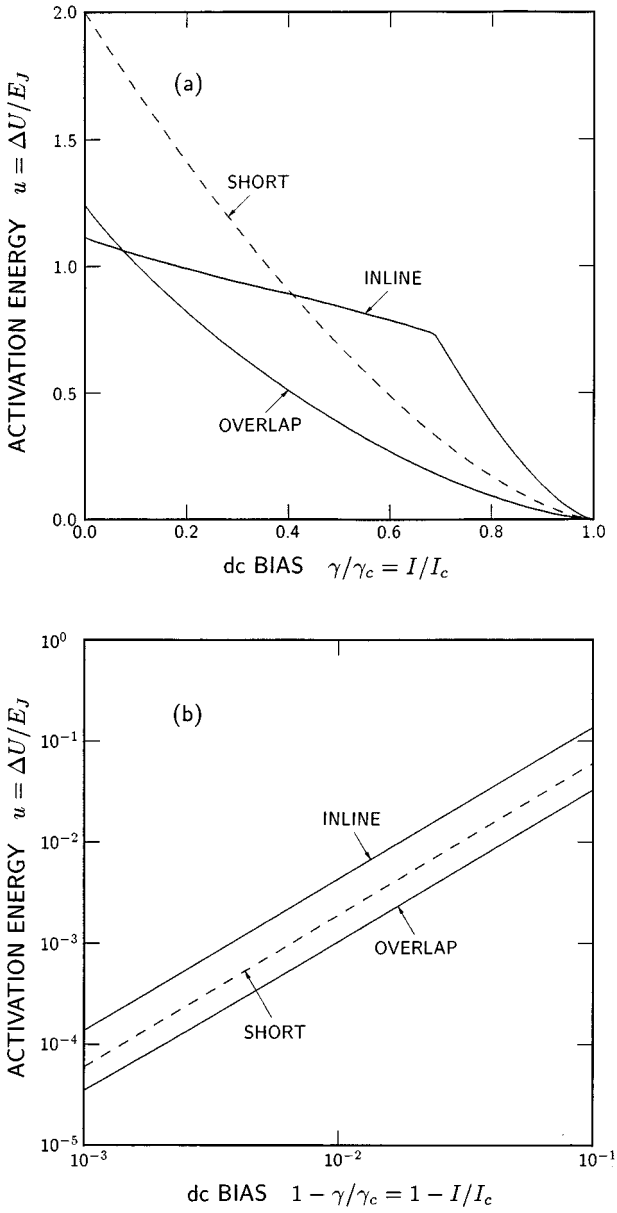

FIG. 7. Activation energy as a function of dc bias for overlap and in-line junctions of length $l=4$ with a magnetic field $\eta=1$ plotted (a) with linear scales and (b) with logarithmic scales. The critical currents for the overlap and in-line junctions are $\gamma_c=0.652$ and 0.727. A dashed line shows the short-junction limit.

The fact that u scales as $(1-\gamma/\gamma_c)^{3/2}$ for long junctions is critical to the analysis of experimental results presented in Sec. IV. Given this scaling, measurements of the escape rate at bias levels near the critical current can be used to deduce the relative activation energy u/u_0 of a long junction compared to a short junction with the same I_c.

D. Attempt frequency

To complete our evaluation of the escape rate $\Gamma=(\omega_A/2\pi)\exp(-\Delta U/k_BT)$ for long junctions, we must calculate the attempt frequency ω_A. According to the general theory of thermally activated escape from multidimensional potentials,[30–32] the attempt frequency for a M-dimensional potential is, in the limit of weak damping,

$$\omega_A=\left(\prod_{m=1}^{M}\omega_{a,m}\right)\left(\prod_{m=1}^{M-1}\omega_{s,m}\right)^{-1}, \tag{23}$$

where the $\omega_{a,m}$ are the M real normal-mode frequencies associated with motion about the potential minimum and the $\omega_{s,m}$ are the $M-1$ real normal-mode frequencies associated with the saddle point. The instability of the saddle point implies that one normal-mode frequency is imaginary, and this mode is omitted from Eq. (23). Provided that a long junction can be modeled as a finite-dimensional system, Eq. (23) can be used to determine the attempt frequency.

To calculate the normal-mode frequencies associated with a given stationary solution $\phi(x')$ of the long junction, we consider the time dependence of an infinitesimal deviation $\Delta\phi(x',t')$ in the absence damping ($\alpha=0$). A finite-dimensional approximation is obtained by expanding $\Delta\phi$ in a truncated cosine series,

$$\Delta\phi(x',t')=\sum_{m=1}^{M}a_m(t')\cos[(m-1)\pi x'/l]. \tag{24}$$

Substituting $\phi(x')+\Delta\phi(x',t')$ into the appropriate equation of motion, either Eq. (3) or (6), we obtain M equations for the coefficients $a_m(t')$ of the form

$$\frac{d^2a_m}{dt'^2}=-\sum_{n=1}^{M}\tilde{A}_{mn}a_n, \tag{25}$$

where the matrix $\tilde{\mathbf{A}}$ is defined by

$$\tilde{A}_{mn}=\left[\frac{(m-1)\pi}{l}\right]^2\delta_{mn}+\frac{2-\delta_{m1}}{l}\times\int_0^l\cos\phi\cos[(m-1)\pi x'/l]\times\cos[(n-1)\pi x'/l]dx'. \tag{26}$$

For a normal mode of oscillation, all of the coefficients a_m have a time dependence of the form $\exp(i\omega t'/\omega_0)$, where ω is the normal-mode frequency. If we define the vector $\mathbf{a}=(a_1,a_2,\ldots,a_M)$, then the equation of motion for a normal mode reduces to

$$\tilde{\mathbf{A}}\mathbf{a}=(\omega/\omega_0)^2\mathbf{a}. \tag{27}$$

Thus, the normal-mode frequencies are related to the eigenvalues μ_m of $\tilde{\mathbf{A}}$ by $\omega_m=\omega_0\sqrt{\mu_m}$.

For junctions up to several times λ_J in length, evaluation of the normal-mode frequencies $\omega_{a,m}$ and $\omega_{s,m}$ requires only a few Fourier components in the expansion of $\Delta\phi$. That is, while $M=10$ was adopted in the calculations presented here, virtually identical results for ω_A were obtained with $M=5$. Thus, our procedure for evaluating the attempt frequency is entirely practical and, combined with that for ΔU, defines the rate of escape from the zero-voltage state of long junctions in the limit $\alpha\ll 1$ and $k_BT\ll\Delta U$.

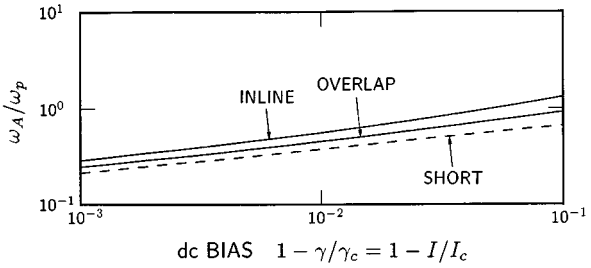

FIG. 8. Attempt frequency as a function of dc bias for overlap and in-line junctions of length $l=4$ with a magnetic field $\eta=1$. A dashed line shows the short-junction limit.

Numerical results for the attempt frequency are presented in Fig. 8 for the overlap and in-line junctions considered previously in Fig. 7. Here, ω_A is normalized to $\omega_p=(2\pi I_c/\Phi_0C)^{1/2}=\omega_0\gamma_c^{1/2}$ to allow comparison with the universal curve, Eq. (14), for the short-junction limit. As with the activation energy, the attempt frequencies for long junctions biased near the critical current differ from the short-junction limit but exhibit the same asymptotic bias dependence for $\gamma\to\gamma_c$. However, because Γ depends linearly rather than exponentially on ω_A, a shift in attempt frequency has a far less dramatic effect on the escape rate than a shift in activation energy. In the analysis of experimental activation energies, we can thus use the short-junction limit for ω_A without significantly affecting the results.

E. Escape near the critical current

For bias currents near the critical current, the activation energy $u=\Delta U/E_J$ for long junctions varies approximately as $(1-\gamma/\gamma_c)^{3/2}$, just as does u_0 for short junctions. Thus, the ratio u/u_0 is nearly independent of the normalized bias γ/γ_c and provides a useful measure of the difference in behavior between long and short junctions near the critical current. This ratio is plotted as a function of magnetic field for overlap junctions of various lengths in Fig. 9. For the purpose of this plot, γ/γ_c was chosen as 0.99, but the results are nearly independent of γ provided $1-\gamma/\gamma_c\ll 1$. Figure 9 also shows the critical current γ_c as a dashed line. The results for $l=0.5$, shown in Fig. 9(a), reveal a threshold curve almost identical to that predicted for a short junction [cf. Eq. (8)]. In this case, u/u_0 is also close to 1, as expected, except at magnetic fields where the critical current is near zero. Over a narrow field range near each minimum in the threshold curve, the activation energy is significantly lower than for a short junction. This result is surprising given that most junction properties approach the short-junction limit closely even for lengths somewhat greater than λ_J. In this regard, the activation energy appears to be an exception, at least near minima of the threshold curve. For longer junctions, the reduction in activation energy becomes greater and extends to wider ranges of magnetic field. As Fig. 9 indicates, thermally activated escape from the zero-voltage state in long junctions differs significantly from the short-junction limit.

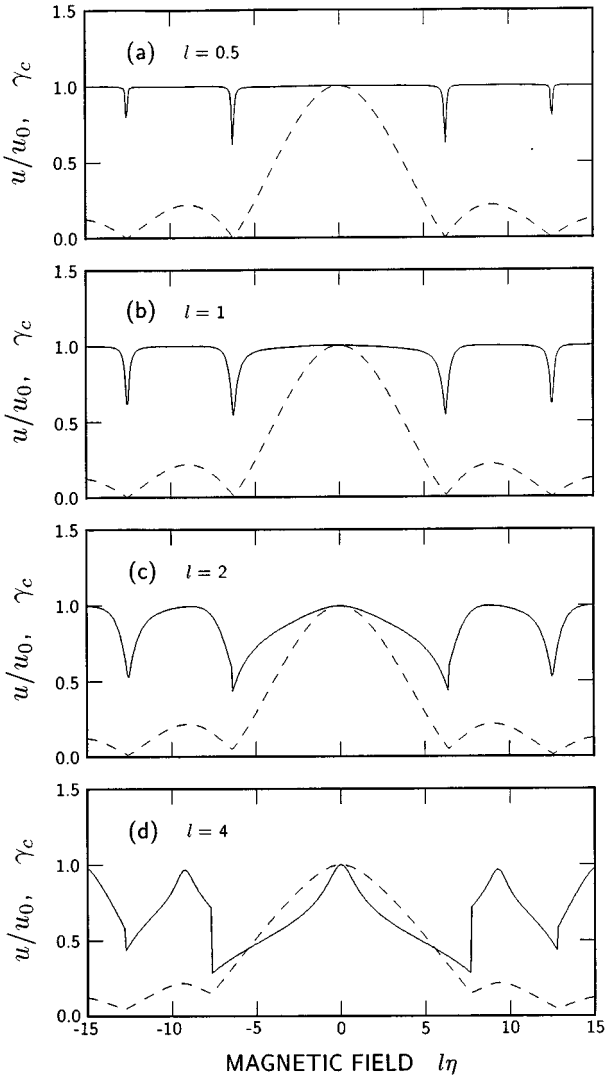

FIG. 9. Activation energy u/u_0 (solid line) and critical current γ_c (dashed line) of a long overlap junction as a function of magnetic field for $\gamma/\gamma_c = 0.99$ and four junction lengths (a) $l = 0.5$, (b) $l = 1$, (c) $l = 2$, and (d) $l = 4$.

Figure 9 also reveals discontinuities in the activation energy at minima in the threshold curve. These discontinuities, most apparent in Figs. 9(c) and 9(d), result because the stable phase configuration near γ_c changes character at the threshold minimum. Near the first minimum of the $l = 4$ curve at $l\eta = 7.7$, these configurations are represented by the two stable stationary solutions shown in Fig. 6(b). For $l\eta < 7.7$, the solution passing through $\phi = 0$ at the midpoint of the junction persists for bias levels up to the critical current and determines the asymptotic activation energy in the limit $\gamma \to \gamma_c$. For $l\eta > 7.7$, however, the solution passing through $\phi = \pi$ at the midpoint persists up to the critical current and determines the asymptotic activation energy. Thus, it is not surprising to find a discontinuity in activation energy at the threshold minimum.

Similar results for the in-line geometry are shown in Fig. 10. As for the overlap geometry, the threshold curve and and activation energy at $l = 0.5$ approach the short-junction limit, and large deviations are found for longer junctions. For the

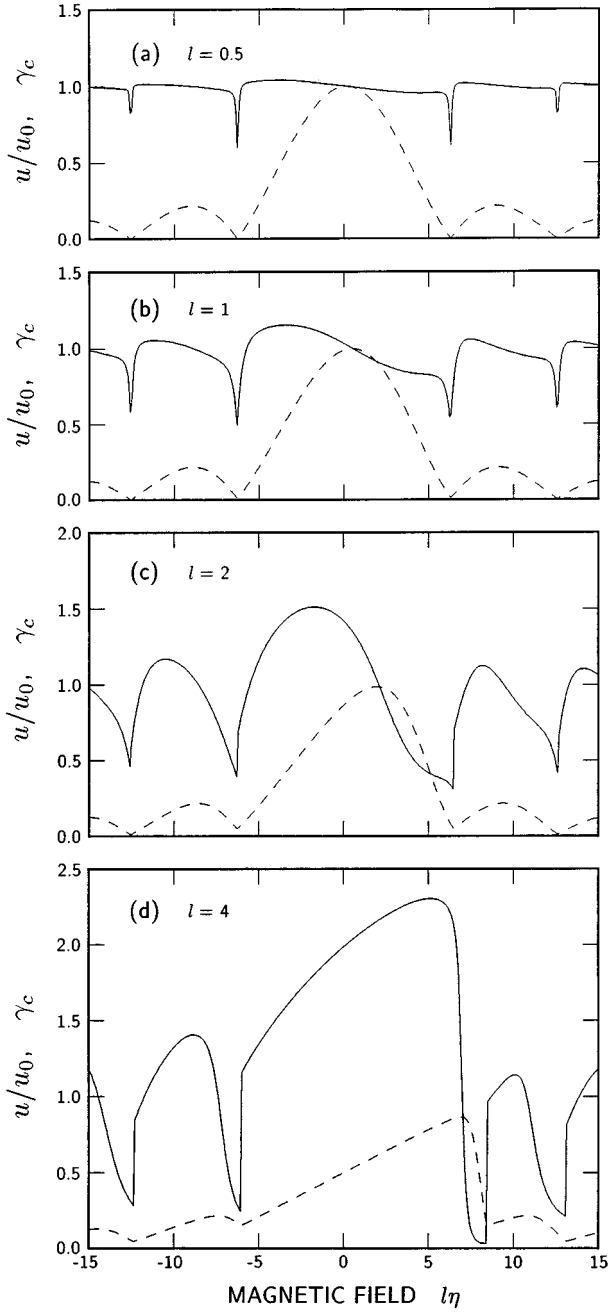

FIG. 10. Activation energy u/u_0 (solid line) and critical current γ_c (dashed line) of a long in-line junction as a function of magnetic field for $\gamma/\gamma_c = 0.99$ and four junction lengths (a) $l = 0.5$, (b) $l = 1$, (c) $l = 2$, and (d) $l = 4$.

in-line geometry, however, the spatial asymmetry of the dc bias results in an asymmetry in both u/u_0 and γ_c with respect to the polarity of the magnetic field. The activation energy is also qualitatively different from the overlap geometry in that u/u_0 exceeds 1 in some instances. All things considered, in-line junctions deviate more strongly from the short-junction limit than overlap junctions.

III. MONTE CARLO SIMULATIONS

As a test of the theory developed above, we have performed Monte Carlo simulations that emulate our experi-

mental measurements of the activation energy for escape from the zero-voltage state. Both the simulations and the experiments consist of a series of trials in which the junction is initialized in the zero-voltage state at $I=0$ and the dc bias is increased at a fixed rate $\dot{I}$ until the junction is observed to switch to the voltage state. Thermal noise induces switching at a bias that varies from trial to trial but is generally somewhat less than the critical current I_c of the noise-free system. Tabulation of the switching current over many trials establishes the probability density $P(I)$, defined such that the $P(I)\Delta I$ is the probability of switching at a bias between I and $I+\Delta I$.

The probability density $P(I)$ can be used to derive an activation energy as follows. First, if ΔI is the width of the current ranges used in tabulating switching events, then the rate of escape from the zero-voltage state at bias I is

$$\Gamma(I)=(\dot{I}/\Delta I)\ln\left[\frac{\int_I^\infty P(I')dI'}{\int_{I+\Delta I}^\infty P(I')dI'}\right]. \tag{28}$$

Given Γ at a particular I and assuming that ω_A is known from Eq. (14), we can calculate the activation energy based on Eq. (1) as $\Delta U=k_BT\ln(\omega_A/2\pi\Gamma)$. However, because the asymptotic bias dependence of ΔU is known, the entire data set can be used to establish u/u_0 with improved accuracy. In this analysis, we consider the function $Y(I)$ defined by

$$\begin{aligned}Y(I)&=[\ln(\omega_A/2\pi\Gamma)]^{2/3}=(\Delta U/k_BT)^{2/3}\\&=[(4\sqrt{2}/3)(E_J/k_BT)(u/u_0)]^{2/3}(1-I/I_c).\end{aligned} \tag{29}$$

The first line of Eq. (29) relates Y to the experimental values of Γ and the estimated the attempt frequency specified by Eq. (14). The last line of Eq. (29), obtained using the asymptotic form of u_0 specified by Eq. (13), defines the relation between Y and u/u_0. In particular, $Y(I)$ varies linearly with I, and the slope dY/dI determines the normalized activation energy according to

$$u/u_0=\frac{3\pi k_BT}{2\sqrt{2}\Phi_0 I_c}|I_c dY/dI|^{3/2}. \tag{30}$$

In addition, the I intercept of $Y(I)$ is the noise-free critical current I_c. Because ω_A depends on I_c, an estimate of I_c must be chosen before $Y(I)$ can be calculated, but iteration quickly leads to a self-consistent value. Thus, analysis of $Y(I)$ allows the determination of both u/u_0 and I_c from Monte Carlo or experimental data.

Monte Carlo simulations were performed for an overlap junction of length $l=2$ represented by the circuit model of Fig. 2(a) with $N=20$ point junctions. Thermal noise was modeled by statistically independent current sources $I_{G/N,i}(t)$ associated with each point junction. Over an integration step Δt, each $I_{G/N,i}(t)$ is represented by its average

$$\overline{I_i}=\frac{1}{\Delta t}\int_t^{t+\Delta t} I_{G/N,i}(t_1)dt_1, \tag{31}$$

which is chosen from a Gaussian random number generator with zero mean and variance

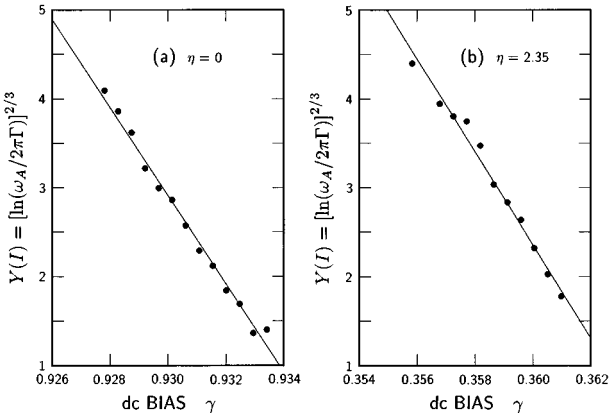

FIG. 11. Logarithmic escape rate Y as a function of dc bias for Monte Carlo simulations of an overlap junction of length $l=2$ (a) in the absence of a magnetic field and (b) for $\eta=2.35$. The simulation assumed a damping coefficient $\alpha=0.05$, a normalized temperature $k_BT/E_0=1.6\times10^{-6}$ and a sweep rate $\dot{I}/\omega_0 I_0=3.7\times10^{-6}$. Calculation of Y is based on 500 switching events.

$$\langle\overline{I_i^2}\rangle=2k_BTG/N\Delta t. \tag{32}$$

In other respects, the circuit simulation proceeds conventionally.

Based on 500 Monte Carlo switching events, the quantity Y is plotted as a function of dc bias for two magnetic fields in Fig. 11. In both cases, Y varies linearly with dc bias, confirming that ΔU scales as $(1-\gamma/\gamma_c)^{3/2}$. Analysis of the data shown in Fig. 11(a) for $\eta=0$ yields $u/u_0=0.93$ and $\gamma_c=0.9358$, in good agreement with the theoretical results $u/u_0=1.00$ and $\gamma_c=1.00$. Similarly, Fig. 11(b) yields $u/u_0=0.60$ and $\gamma_c=0.3642$ for $\eta=2.35$, in rough agreement with the theoretical results $u/u_0=0.76$ and $\gamma_c=0.35$. Thus, although limited in accuracy by statistics, the Monte Carlo simulations confirm the basic validity of our theoretical approach.

IV. EXPERIMENT

The measurement system used to determine the probability of escape from the zero-voltage state is illustrated in Fig. 12. To avoid an enhancement of the escape rate due to environmental noise, the junction is shielded by placing it inside a copper box, and all leads entering the box are filtered. The *R-C-R* filters consist of 1-kΩ surface-mount resistors, placed as close to the junction chip as possible, and 5-nF feedthrough capacitors. Twisted pairs of phosphor-bronze wire connect the chip to external electronics. This shielding was tested in earlier experiments,[41] which recorded intrinsic temperatures as low as 0.3 K.

Escape rates are measured using a ramp generator to provide a current bias that increases from 0 at a rate $\dot{I}$, while a comparator circuit determines when the junction voltage exceeds a preset threshold and triggers the data acquisition computer to record the bias current at which switching occurred. The sweep rate $\dot{I}$ is typically between 20 and 200 mA/s, and a 16-bit analog-to-digital converter is used to read the bias current. The experiment is repeated under computer

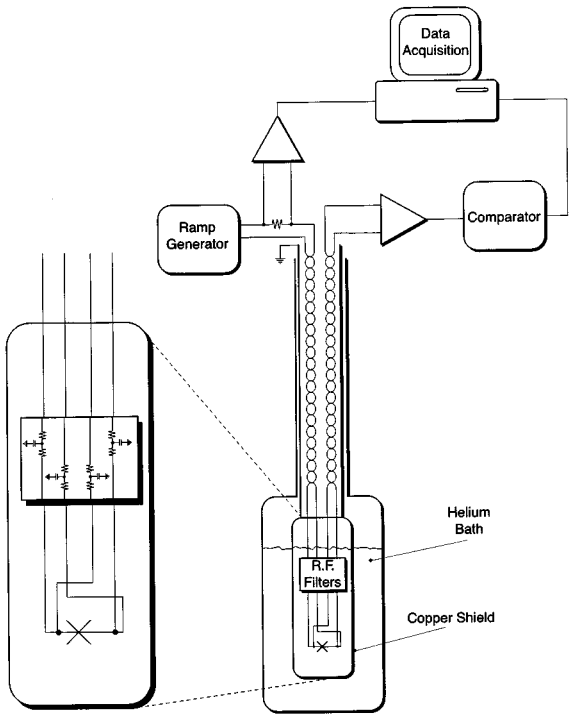

FIG. 12. Measurement system used to determine the probability of escape from the zero-voltage state as a function of dc bias.

control to obtain about 10^4 values of switching current in a time ranging from tens of seconds to a few minutes, depending of the sweep rate. The current values are sorted into about 100 channels to form a histogram that represents the probability of escape as a function of current. This histogram is then used to compute the rate of escape $\Gamma(I)$ from Eq. (28). Fitting $Y(I)=[\ln(\omega_A/2\pi\Gamma)]^{2/3}$ with a straight line gives the activation energy (from the slope) and the noise-free critical current (from the $Y=0$ intercept).

Detailed measurements of escape rates were made for two long junctions, a Nb-AlO_x-Nb trilayer junction with an overlap geometry and a Nb-NbO_x-PbInAu window junction with an in-line geometry.

The Nb-AlO_x-Nb overlap junction was fabricated with a standard trilayer process,[41] in which Nb is deposited by dc-magnetron sputtering and the barrier is grown by thermal oxidation of an aluminum layer in pure oxygen. The junction is patterned by reactive ion etching of the top electrode and sealed by a self-aligned layer of thermally evaporated silicon monoxide. The wiring layer is sputtered Nb, deposited after an *in situ* sputter etch. The quality of these junctions expressed by V_m (the critical current times the subgap resistance at 2 mV) ranges between 50 and 70 mV at 4.2 K.

Escape rates were recorded for an overlap junction that measured 4 μm by 70 μm and had a critical current of 1.07 mA at zero field. From the threshold curve of a small junction on the same chip, we estimate $\lambda_J=30\pm5$ μm, and from the position of the Fiske resonances the specific capacitance is $C_s=0.05\pm0.01$ F/m^2. Thus, the normalized length of the junction is roughly $l=L/\lambda_J=2.3$, the total capacitance is $C=14$ pF, the critical-current density is $J_c=380$ A/cm^2, and the zero-field plasma frequency is $\omega_0/2\pi=77$ GHz. From

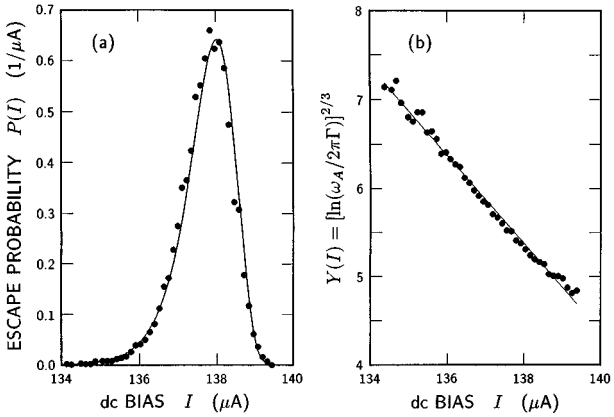

FIG. 13. (a) Probability density for escape from the zero-voltage state and (b) logarithmic escape rate as a function of dc bias, based on measurements of 10^4 switching events in the Nb-AlO_x-Nb overlap junction at 4.2 K, subject to a magnetic field of 0.07 mT. Solid lines are theory curves for the short-junction limit modified to reflect the value of u/u_0 inferred from the experimental $Y(I)$.

the measured V_m of 50 mV, we estimate a damping parameter of $\alpha=0.003$.

Typical results for the escape probability at 4.2 K are shown in Fig. 13(a) as a function of dc bias for the overlap junction in a magnetic field of 0.07 mT. Solid circles show experimental results based on the observation of 10^4 switching events. When converted to an escape rate using Eq. (28), the escape data yield the function $Y(I)$ plotted in Fig. 13(b). The linear dependence of $Y(I)$ on current indicates that the activation energy scales as $(1-I/I_c)^{3/2}$. However, calculations based on the measured $Y(I)$ yield a normalized activation energy of $u/u_0=0.40$. When expressions for the short-junction limit are modified to reflect the measured u/u_0 and I_c, we obtain the theory curves shown as solid lines in Figs. 13(a) and 13(b). Thus, while the activation energy scales with current as in a short junction, its magnitude is significantly less than for a short junction. These results are in qualitative agreement with the theory of long junctions developed in Sec. II.

A more detailed comparison between theory and experiment for the overlap junction is shown in Fig. 14. Here, solid circles indicate experimental results and dashed lines correspond to the theory developed in Sec. II. Figure 14(a) shows the experimental and theoretical threshold curves. The agreement evident here is the result of scaling the theoretical currents to match the observed maximum I_c, scaling the theoretical magnetic field to match the location of the first minimum, and adjusting the theoretical junction length to obtain the best fit to the secondary maxima. The resulting length of $l=2.5$ is in good agreement with the value of $l=2.3$ obtained independently. No additional parameters were adjusted to obtain the fit between theory and experiment for the activation energies plotted in Fig. 14(b). Considering the difficulty of the experiment, the observed quantitative agreement with theory is remarkable. In particular, the maximum and minimum values of u/u_0 are nearly the same in theory and experiment, the general shapes of the curves are in good agreement, and discontinuities in the theoretical activation energy at minima in the threshold

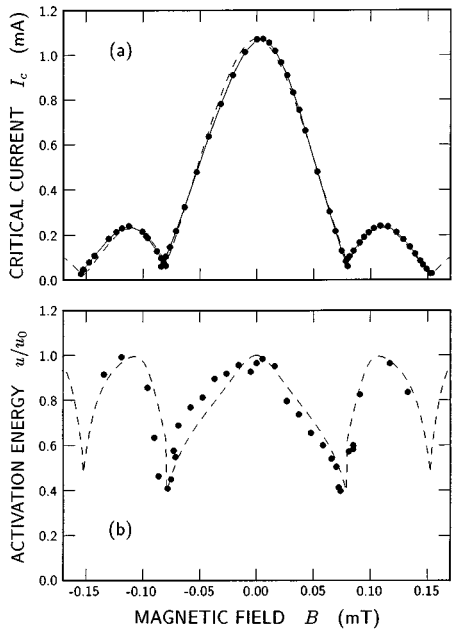

FIG. 14. (a) Critical current and (b) activation energy as a function of magnetic field for the Nb-AlO_x-Nb overlap junction at 4.2 K. Solid circles show experimental results and dashed lines show theoretical predictions for a junction length of $l=2.5$.

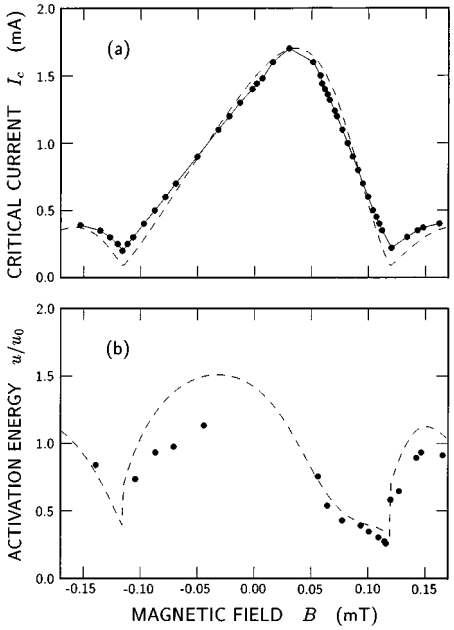

FIG. 15. (a) Critical current and (b) activation energy as a function of magnetic field for the Nb-NbO_x-PbInAu in-line junction at 4.2 K. Solid circles show experimental results and dashed lines show theoretical predictions for a junction length of $l=2$.

curve are apparently reflected in the experimental data. These points of agreement leave little doubt that long-junction effects play a major role in determining the activation energy for escape from the zero-voltage state in this junction.

The Nb-NbO_x-PbInAu in-line junction was fabricated using a standard technique,[42] in which the barrier is formed by plasma oxidation and the junction area is determined by a SiO window. The in-line junction measured 3 μm by 60 μm and had a maximum observed critical current of 1.7 mA. Based on the presence of a Fiske step at 130 μV and the measured capacitance of similar junctions,[43] we estimate a specific capacitance of $C_s=0.13$ F/m^2 and a Josephson penetration depth of $\lambda_J=20$ μm. Thus, the normalized length of the in-line junction is roughly $l=3$, the total capacitance is $C=23$ pF, and the zero-field plasma frequency is $\omega_0/2\pi=75$ GHz. From the measured V_m of 20 mV, we estimate a damping parameter of $\alpha=0.008$.

A comparison between experiment and theory for the in-line junction is presented in Fig. 15. The theoretical threshold curve shown by the dashed line in Fig. 15(a) was obtained by scaling the theoretical curve in current and field to match the observed maximum critical current and the field values of the critical-current minima and by adjusting the normalized length to fit the observed asymmetry. The required length was $l=2$, or about 2/3 of the calculated value. This discrepancy probably derives from the fact that the junction area is defined by a window in a dielectric layer deposited between the base and counter electrodes. The window geometry leads to a superconducting frame surrounding the junction that allows bias current to enter the junction along its entire length, not just at the ends, as assumed in the idealized model of Fig. 1(b). Because the bias current is more uniformly distributed, the asymmetry of the observed threshold curve is not as great as would be expected for an ideal in-line junction of length $l=3$.

Even though our idealized model does not strictly apply to the experimental junction, we compare the observed activation energy with theory in Fig. 15(b). Again, no additional parameters were adjusted to obtain the fit shown here. Although agreement between theory and experiment is not as quantitative as for the overlap junction, the curves are qualitatively similar in many respects. In particular, the predicted discontinuity in u/u_0 at the threshold minimum near 0.12 mT is clearly reflected in the experimental data. The strongest disagreement is found at negative fields, where theory predicts values of u/u_0 substantially greater than 1. Although some data points are missing in this region due to limitations of the apparatus in recording large currents, the experimental points clearly fail to reach the high values of u/u_0 predicted by theory. One data point does, however, fall marginally above $u/u_0=1$. Taken together, the points of agreement found in Fig. 15 are substantial in spite of the limited applicability of our model and add weight to the idea that the activation energy for thermally induced escape from the zero-voltage state is strongly influenced by long-junction effects.

ACKNOWLEDGMENTS

The Italian portion of this work was supported by the Istituto Nazionale di Fisica Nucleare through the Macroscopic Quantum Coherence Project. Helpful and stimulating discussions with R. Cristiano, L. Frunzio, R. Leoni, and J. M. Martinis were important in the development of this research program. Junctions were fabricated at IESS, CNR in Rome.

*Also affiliated with Istituto Nazionale di Fisica Nucleare, Italy.
[1] H. A. Kramers, Physica **7**, 284 (1940).
[2] T. A. Fulton and L. N. Dunkleberger, Phys. Rev. B **9**, 4760 (1974).
[3] Y. M. Ivanchenko and L. A. Zil'berman, Pis'ma Zh. Eksp. Teor. Fiz. **8**, 189 (1968) [JETP Lett. **8**, 113 (1968)]; Zh. Eksp. Teor. Fiz. **55**, 2395 (1968) [Sov. Phys. JETP **28**, 1272 (1969)].
[4] V. Ambegaokar and B. I. Halperin, Phys. Rev. Lett. **22**, 1364 (1969).
[5] A. C. Biswas and S. S. Jha, Phys. Rev. B **2**, 2543 (1970).
[6] M. Büttiker, E. P. Harris, and R. Landauer, Phys. Rev. B **28**, 1268 (1983).
[7] V. I. Mel'nikov, Zh. Eksp. Teor. Fiz. **88**, 1429 (1985) [Sov. Phys. JETP **61**, 855 (1985)].
[8] A. Barone, R. Cristiano, and P. Silvestrini, J. Appl. Phys. **58**, 3822 (1985).
[9] R. Cristiano and P. Silvestrini, J. Appl. Phys. **60**, 3243 (1986).
[10] M. H. Devoret, J. M. Martinis, D. Esteve, and J. Clarke, Phys. Rev. Lett. **53**, 1260 (1984).
[11] P. Silvestrini, O. Liengme, and K. E. Gray, Phys. Rev. B **37**, 1525 (1988).
[12] P. Silvestrini, S. Pagano, R. Cristiano, O. Liengme, and K. E. Gray, Phys. Rev. Lett. **60**, 844 (1988).
[13] J. R. Kirtley, C. D. Tesche, W. J. Gallagher, A. W. Kleinsasser, R. L. Sandstrom, S. I. Raider, and M. P. A. Fisher, Phys. Rev. Lett. **61**, 2372 (1988).
[14] E. Turlot, D. Esteve, C. Urbina, J. M. Martinis, M. H. Devoret, S. Linkwitz, and H. Grabert, Phys. Rev. Lett. **62**, 1788 (1989).
[15] P. Silvestrini, Phys. Rev. B **46**, 5470 (1992).
[16] R. F. Voss and R. A. Webb, Phys. Rev. Lett. **47**, 265 (1981).
[17] L. D. Jackel, J. P. Gordon, E. L. Hu, R. E. Howard, L. A. Fetter, D. M. Tennant, R. W. Epworth, and J. Kurkijärvi, Phys. Rev. Lett. **47**, 697 (1981).
[18] S. Washburn, R. A. Webb, R. F. Voss, and S. M. Faris, Phys. Rev. Lett. **54**, 2712 (1985).
[19] M. H. Devoret, J. M. Martinis, and J. Clarke, Phys. Rev. Lett. **55**, 1908 (1985).
[20] J. M. Martinis, M. H. Devoret, and J. Clarke, Phys. Rev. B **35**, 4682 (1987).
[21] J. M. Martinis, M. H. Devoret, and J. Clarke, Phys. Rev. Lett. **55**, 1543 (1985).
[22] D. Esteve, M. Devoret, and J. M. Martinis, Phys. Rev. B **34**, 158 (1986).
[23] P. Silvestrini, Y. N. Ovchinnikov, and R. Cristiano, Phys. Rev. B **41**, 7341 (1990).
[24] P. Silvestrini, Phys. Lett. A **152**, 306 (1991).
[25] C. D. Tesche, J. Low Temp. Phys. **44**, 119 (1981).
[26] M. Naor, C. D. Tesche, and M. B. Ketchen, Appl. Phys. Lett. **41**, 202 (1982).
[27] E. Ben-Jacob, D. J. Bergman, Y. Imry, B. J. Matkowsky, and Z. Schuss, J. Appl. Phys. **54**, 6533 (1983).
[28] F. Sharifi, J. L. Gavilano, and D. J. Van Harlingen, Phys. Rev. Lett. **61**, 742 (1988); IEEE Trans. Magn. **MAG-25**, 1174 (1989).
[29] S. Han, J. Lapointe, and J. E. Lukens, Phys. Rev. Lett. **63**, 1712 (1989); Phys. Rev. B **46**, 6338 (1992).
[30] H. C. Brinkman, Physica **22**, 149 (1956).
[31] R. Landauer and J. A. Swanson, Phys. Rev. **121**, 1668 (1961).
[32] P. Hänggi, P. Talkner, and M. Borkovec, Rev. Mod. Phys. **62**, 251 (1990).
[33] N. F. Pedersen, in *Solitons*, edited by A. A. Maradudin and V. H. Agranowich (North-Holland, Amsterdam, 1986), p. 469.
[34] R. D. Parmentier, in *The New Superconducting Electronics*, edited by H. Weinstock and R. W. Ralston (Kluwer, Dordrecht, 1993), p. 221.
[35] K. Hida and U. Eckern, Phys. Rev. B **30**, 4096 (1984).
[36] K. Hida, Z. Phys. B **61**, 223 (1985).
[37] S. Nakaya and K. Hida, J. Phys. Soc. Jpn. **55**, 3768 (1986).
[38] H. Simanjuntak and L. Gunther, Phys. Rev. B **42**, 930 (1990).
[39] A. Barone and G. Paternò, *Physics and Applications of the Josephson Effect* (Wiley, New York, 1982).
[40] S. Basavaiah and R. F. Broom, IEEE Trans. Magn. **MAG-11**, 759 (1975).
[41] C. Cosmelli, G. Diambrini−Palazzi, F Chiarello, A. Costantini, M. G. Castellano, R. Leoni, G. Torrioli, P. Carellim, R. Cristiano, and L. Frunzio, in *Applied Superconductivity 1995*, edited by D. Dew-Hughes (Institute of Physics, Bristol, 1995), Vol. 2, p. 1323.
[42] R. F. Broom, S. I. Raider, A. Oosenbrug, R. E. Drake, and W. Walter, IEEE Trans. Electron Devices **ED-27**, 1998 (1980).
[43] J. H. Magerlein, IEEE Trans. Magn. **MAG-17**, 286 (1981).